ADVANCED OPTICAL MATERIALS

www.advopticalmat.de

Direct Light-Writing of Nanoparticle-Based Metallo-Dielectric Optical Waveguide Arrays Over Silicon Solar Cells for Wide-Angle Light Collecting Modules

*Saeid Biria, Thomas S. Wilhelm, Parsian K. Mohseni, and Ian D. Hosein**

Here presented are the properties and performance of a new metallo-dielectric waveguide array structure as the encapsulation material for silicon solar cells. The arrays are produced through light-induced self-writing combined with in situ photochemical synthesis of silver nanoparticles. Each waveguide comprises a cylindrical core consisting of a high refractive index polymer and silver nanoparticles homogenously dispersed in its medium, all of which are surrounded by a low refractive index common cladding. The waveguide array-based films are processed directly over a silicon solar cell. Arrays with systematically varied concentration of $AgSbF_6$ as the salt precursor are explored. The structures are tested for their wide-angle light capture capabilities, specifically toward enhanced conversion efficiency and current production of encapsulated solar cells. Observed are increases in the external quantum efficiency, especially at wide incident angles up to 70°, and nominal increases in the short circuit current density by 1 mA cm^{-2} (relative to an array without nanoparticles). Enhanced light collection is explained in terms of the beneficial effect of scattering by the nanoparticles along the waveguide cores. This is a promising approach toward solar cell encapsulants that aid to increase solar cell output over both the course of the day and year.

1. Introduction

The increasing dominance of photovoltaic modules for energy conversion and its decreasing manufacturing costs has placed an imperative that any approach to further increase performance must keep costs low and be easily integrated into current manufacturing chains. One of the most low-cost and effective approaches to increase light capture and conversion is through engineering light management structures into the encapsulant materials, whose general purpose is to protect the solar cell. Optical structures explored thus far include nanoparticle surface coatings,[1] nanostructured diffractive, diffuse, and scattering layers,[2] nanotexturing,[3] geometric optical structures,[2b,4] contact cloaking,[5] and back-contact architectures.[6]

Particularly, the application of nanoparticles as diffuse scattering components is quite attractive, owing to the simplicity of their incorporation into the encapsulation layer through straightforward coating methods. Their generally agreed mechanism for enabling greater enhancement is via scattering light beyond the "loss cone" as well as mitigation of losses from the metallic front contacts. Glass and polymer nanoparticles have been used to this end, commonly as a top coating to a glass or polymer encapsulant already overlaid on the solar cell. Silver is also attractive as it has relatively low parasitic absorption, and it is commonly incorporated either as a coating directly on the solar cell surface, or in the buffer or active layer of the solar cell.[7] In this way, its capability to provide enhancement is through effects such as plasmon resonance, near-field coupling, and energy transfer via the generation of "hot" electrons.[7] For example, a monolayer of silver nanoparticles with at least a 10% surface coverage will interact with all incident light, enabling broadband usage.[8] Silver nanoparticles also efficiently scatter incident photons, and this effect has been leveraged to increase the path length of light to increase the likelihood of absorption, especially in thin-solar cells.[9] Relatively smaller particle sizes result in more forward scattering,[10] and this process can be used to redirect light to different directions from which it initially entered the solar cell.[11] The general consensus is that multiple scattering by the nanoparticles can improve external quantum efficiency (EQE), and this general operational behavior is characterized as "light trapping" or a "far-field effect."[12] However, little has been explored with regards to the incorporation of silver nanoparticles embedded in the encapsulation materials (i.e., not in contact with the solar cell surface, nor in the solar cell materials). When incorporated into an encapsulant, it is expected that for very small silver nanoparticles sizes (<50 nm) the surface plasmon resonance is shifted into the UV (or deep blue), allowing them to behave as very low-loss scattering centers. Hence, a silver nanoparticle composite encapsulant is an interesting materials system to explore.

S. Biria, Prof. I. D. Hosein
Department of Biomedical and Chemical Engineering
Syracuse University
Syracuse, NY 13244, USA
E-mail: idhosein@syr.edu
T. S. Wilhelm, Prof. P. K. Mohseni
Rochester Institute of Technology
Microsystems Engineering and NanoPower Research Laboratories
Rochester, NY 14623, USA
The ORCID identification number(s) for the author(s) of this article can be found under https://doi.org/10.1002/adom.201900661.

DOI: 10.1002/adom.201900661

We recently demonstrated the capability for polymer waveguide arrays to enhance nonnormally incident light collection.[13] The waveguide arrays are produced in a photo-reactive blend of high and low refractive index polymers irradiated with arrays of microscale optical beams. Each beam undergoes self-trapping owing to photopolymerization-induced optical nonlinearity, resulting in divergence-free propagation of the beams across the medium.[14] The sustained polymerization in the regions of the optical beams results in photopolymerization-induced phase separation of the low-index polymer into the surrounding dark regions, thereby producing the core-cladding architecture with cylindrical geometry, namely, a microscale fiber optic. When overlaid on a solar cell, nonnormally incident light can be collected within the acceptance cone of the waveguides, leading to greater light collection and conversion, as compared with a uniform encapsulant. This enhancement originates from converting nonnormally incident light to quasi-normally incident light, which specifically mitigates contact shading,[15] an effect exacerbated at greater incident angles. However, to further enhance light collection beyond that dictated by waveguide optics, stronger light-matter interactions are needed.

In this work, metallo-dielectric waveguide array structures are produced by combining light-induced self-writing in a two-component photopolymerizable blend[14] with concurrent in situ synthesis of silver nanoparticles via photo-reduction of a silver salt ($AgSbF_6$).[16] The waveguide array structures are processed directly over a silicon solar cell via casting the precursor resin and then irradiating the resin from above with an array of microscale UV optical beams, which undergo self-trapping, making the approach easily integrated into the processing of modules. Irradiation with an array of UV beams creates periodic waveguide array architectures with the waveguide cores consisting of a homogenous distribution of silver nanoparticles. Our strategy herein is to leverage the waveguide array to provide a baseline structure for a wider light acceptance window,[13,17] which already performs better than a uniform encapsulant, and for the in situ synthesized nanoparticles to impart further optical functionality—through light scattering—thereby enhancing the collection of light (both normally and nonnormally incident) through a synergy between light-guiding and light scattering. We systematically vary the $AgSbF_6$ content to produce waveguide cores with different silver nanoparticle concentrations, and investigate as a function of $AgSbF_6$ concentration performance enhancements specifically in terms of the EQE and current density. We show that for specific concentrations, there is an increase in the EQE over the angular range (0°–70°) and nominal increases in the current density of up to 1 mA cm^{-2}. Our enhancements achieved herein (up to 9.9% increase in short circuit current density) are also greater than those of other approaches which show generally a 1–3% enhancement.[5a,18] Advantageously, preparing the structures from a single photocurable formulation aligns with the imperative to maintain the approach as straightforward and easily integrated into manufacturing solar cell modules. The combination of light self-trapping and photoreduction of the silver salt enables the nanoparticle formation specifically in the desired high index regions of the structure. The novelty of this work is in the incorporation of silver nanoparticles in the encapsulation material of a solar cell, which is different from previous works that incorporate them on the solar cell surface, or in the buffer or active layer. The capability to directly process the metallo-dielectric waveguides over the solar cell surface is also an advance in the fabrication method.

2. Results and Discussion

Figure 1a illustrates the process of directly synthesizing the metallo-dielectric waveguide arrays over the solar cell surface, which entails casting the resin formulation over its surface, followed by irradiation with the array of UV beams, which facilitates the polymerization of cylindrical cores, phase separation of the two component blend to form the core-cladding architecture with cylindrical geometry, and concurrent photoreduction of the $AgSbF_6$ into $Ag^0_{(s)}$. As shown in Figure 1b, the result is a vast array of periodically spaced cylindrical waveguides located

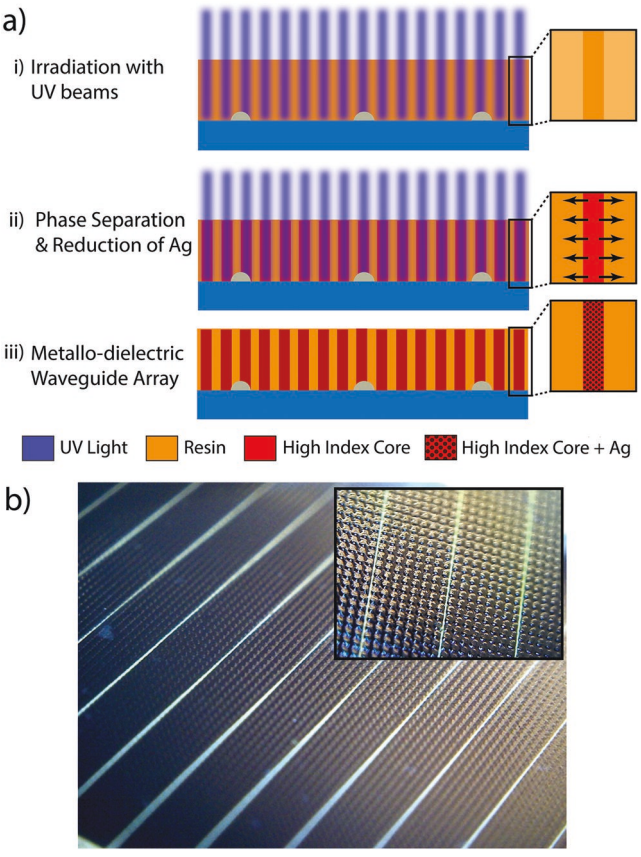

Figure 1. a) Schematic of the fabrication of metallo-dielectric waveguide arrays directly over a silicon solar cell surface. The process of material formation is as follows: i) The polymer blend resin consisting of the silver salt is cast over the surface, and irradiated with an array of UV optical beams that initiate the polymerization of cylindrical cores, ii) with continued irradiation, phase separation of the low index polymer into nonirradiated regions occurs (indicated by the arrows), iii) finally concurrent and continued photoreduction of silver nanoparticles in the irradiated regions. b) Macro-lens optical image of the large-scale, defect-free waveguide array consisting of vertically aligned cylindrical waveguides over the solar cell surface. Silvery parallel lines are the top contacts (spacing = 2.375 mm). Inset shows a higher magnification image of the array.

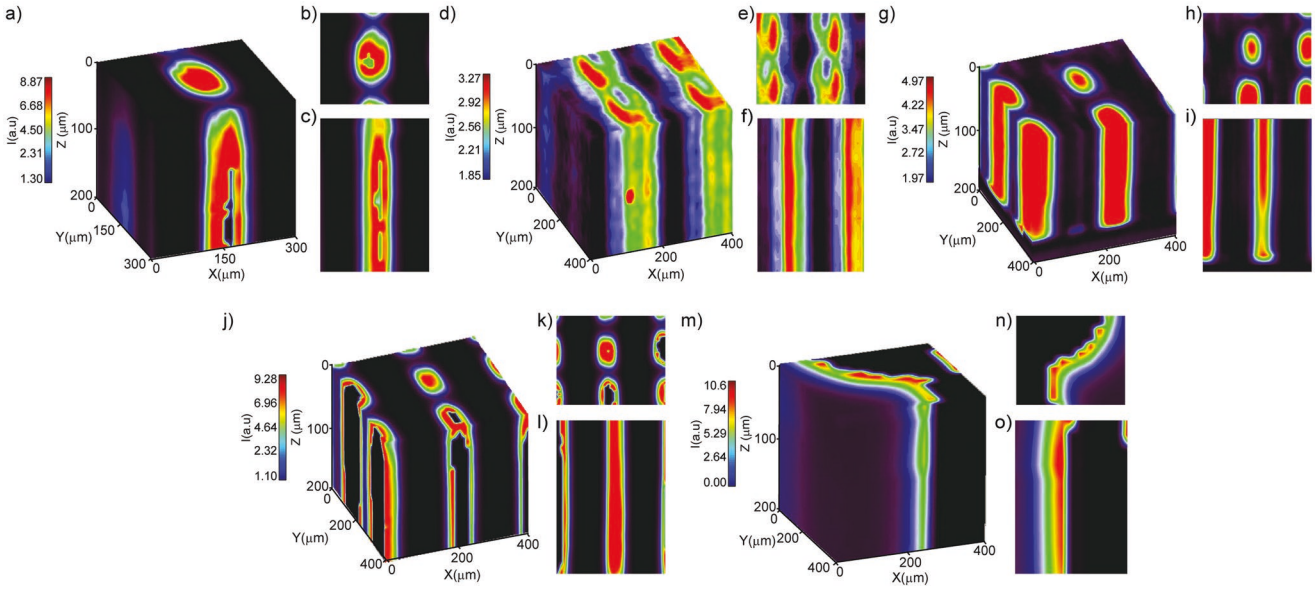

Figure 2. Raman volume map of self-written waveguides with a,d,g,j,m) 0.1%, 0.5%, 1.0%, 2.0%, and 3% of $AgSbF_6$, respectively. b,e,h,k,n) *xy*-slices through the middle of the waveguides, revealing their transverse cross-sectional profiles. c,f,i,l,o) *yz*-slices through the core central axis, revealing their longitudinal profiles that extend over the depth of the film. Red zones indicate regions in the sample comprising the silver nanoparticles. Black color in the center of the waveguides is an artifact of signal saturation.

in the area between the front contacts of the solar cell. There was no deleterious effect from the reflective contacts on the fabrication process (i.e., possible back reflection of UV light, scattering, etc.). Rather, lines of waveguides could also be observed to form over the contacts, or with a simple shift to the optical mask they could be ensured to form between the contacts. This is a critical result, which ensures the quality of the processed coatings, and optimal functionality in the collection of light. Hence, based on the alignment position of the mask, the waveguides can form over the contacts, or if properly aligned, the contacts lie in the spacing between the waveguides.

Figure 2 shows Raman volume maps which reveal the spatial location of the nanoparticles in the waveguide arrays. Higher intensities reveal regions with higher concentration of silver nanoparticles, owing to Raman peaks' concentration dependent intensity. Notably, the silver nanoparticles are located solely in the waveguide cores, as expected owing to these being the regions of high illumination by the optical beams. The distribution of the nanoparticles appears uniform over the length of the cylindrical cores, and the concentration slightly tapers at the peripheries in accordance with the decrease in intensity of light which is confined to the inscribed waveguide during the fabrication process. Furthermore, there is no observation of phase separation of the nanoparticles into the interstitial space (i.e., the low index surroundings). This is most likely due to the silver nanoparticles forming under conditions in which the high-index core (NOA65) is highly crosslinked, and thus cannot easily diffuse out of the cores, yet the Ag salt precursor can diffuse from the dark regions into the bright to facilitate their consumption and continued growth of the particles.

The ability to capture and transmit optical energy incident over a wide range of angles relative to the waveguide core axes is shown in **Figure 3**. Preservation of the optical intensity located at the exit points of the individual waveguides is clearly observed. Notably light is more tightly confined in a sample with Ag nanoparticles, especially with increasing incident angles, as compared to a regular waveguide array (i.e., 0 wt% $AgSbF_6$). Even at very high angles of incidence (60°–70°) the confinement

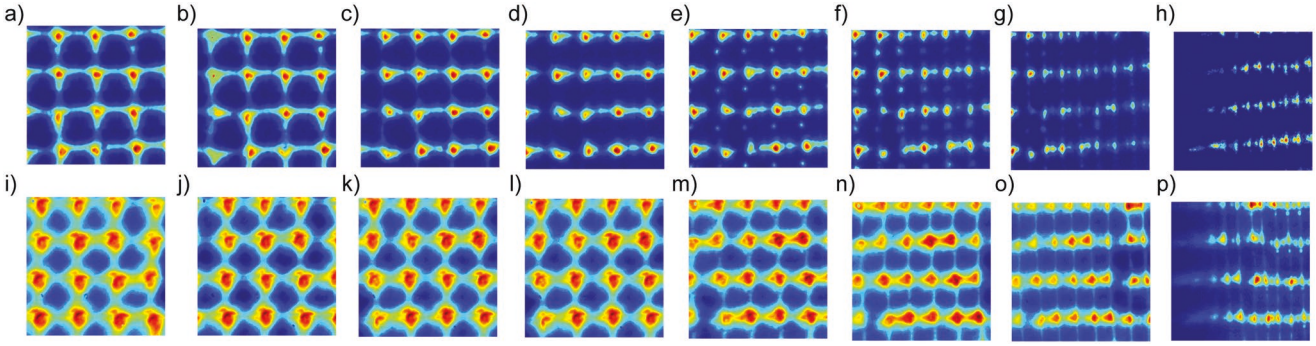

Figure 3. CCD images of the transverse intensity profile of the waveguide arrays from angles 0° to 70° (left to right in 10° increments) for a–h) a metallo-dielectric waveguide array (0.5 wt% $AgSbF_6$) and i–p) a dielectric waveguide array (i.e., no $AgSbF_6$).

and transmission of light in the individual waveguides can be clearly observed for the metallo-dielectric waveguide array. Whereas, the "smearing" in the spatial intensity profile for the regular waveguide array is indicative of light not being strongly confined to the individual waveguides, and consequently light can cut across them. Hence, the advantage of synthesizing nanoparticles in the cores is that, over a wider range of incident angles, the optical transmission retains a quasi-normally incident propagation direction within the waveguide array and will impinge on the underlying solar cell this way.

Previous work on the photoreduction of noble metal nanoparticles shows their size to be around 10–50 nm, such that the plasmon absorbance peak of the silver nanoparticles is in the UV range, within the strong absorbance region of the polymer, and thus cannot be discerned (see Supporting Information). However, any expected plasmon absorbance is also below the operational wavelength range of the solar cell, and is thus not deleterious to its operation (vide infra). All of the samples were transparent, which indicates that metallic particles in the 10 s of nanometers in diameter had formed, which has been confirmed previously with samples photocured at the same intensity (as well as similar salt, $AgSbF_6$, and photoinitiator concentrations, 1–5% and 2%, respectively).[16,19] The decreasing transmission around 350–375 nm is associated with the greater UV absorbance of the nanoparticles with its increasing concentration in samples. Optical microscopy (Figure 1) also indicates that the nanoparticles are well dispersed in the cores (which is corroborated by Raman mapping), with no significant macroscopic agglomerates. **Figure 4**a shows transmission spectra of the waveguide array structures as a function of the different weight percentages of $AgSbF_6$. Highly transparent samples in the visible and near-infrared regions are produced. Figure 4b shows refractive index measurements of uniformly cured slabs of NOA65 with systematically varied $AgSbF_6$ concentrations, as a means to measure in bulk the expected refractive index of the waveguide core. There is a drop in the refractive index, owing to the slight decrease in conversion of the polymer with increased $AgSbF_6$ concentration, as this conversion to higher molecular weight is what causes the higher refractive index of the polymer.[20] The waveguide acceptance range ($\Delta\theta$) is calculated based on the refractive index of the core (n_1) and the surroundings (i.e., cladding) (n_2) according to $\sin(\Delta\theta/2) = \sqrt{n_1^2 - n_2^2}$.[21] Using the refractive index values of the polymers (NOA65: 1.653, PDMS:1.412),[13a] a maximum acceptance range of 30° is possible. It is above this value that light is observed to begin "leaking" out of the waveguide cores (contrast Figure 3e to h with m to p). The drop in refractive index with increased weight percent of $AgSbF_6$ is quite small (0.003) such that the theoretical angular acceptance range is essentially based on the refractive index difference between the core (NOA65) and cladding (polydimethylsiloxane (PDMS)). Hence, rather than refractive index changes, the main mechanism by which the nanoparticles enhance the waveguides is most likely through a stronger confinement effect or favorable scattering that retains light within the cores.

We hereon compare the solar cell performances of the metallo-dielectric waveguides relative to waveguides with no silver nanoparticles (i.e., 0 wt%), which has been established to widen the acceptance range relative to a uniform encapsulant.[13a] **Figure 5** shows EQE measurements of encapsulated solar cells for the range of $AgSbF_6$ concentrations explored. One observation is the lesser drop in the EQE when employing metallo-dielectric waveguides relative to regular waveguides, especially for wide incident angles $\theta_{inc} > 40°$. The EQE drops the least with increased incident angle for the sample with 0.5 wt% $AgSbF_6$ (Figure 5c). Specifically, for directly processed resins, two key observations are notable. First, the drop in the EQE for a regular waveguide array is less than for that produced through lamination (see Supporting Information), indicating that direct processing provides better efficiency performance. This might be explained by the interface between the resin and the silicone priming layer used to planarize the silicon solar cell surface, which can cause additional back reflection of light which may be lost from the cell. Second, smaller drops in EQE are observed with the metallo-dielectric waveguides directly processed over the solar cell. There is no clearly discernable wt% of $AgSbF_6$ as the champion for enhancement of efficiency; 0.5 wt% $AgSbF_6$ shows nominally the greatest abatement in the drop in EQE, specifically assessed within the visible region of the spectra ($\lambda \sim 725$ nm), yet all weight fractions lead to relatively comparable enhancement across the wavelength spectrum examined.

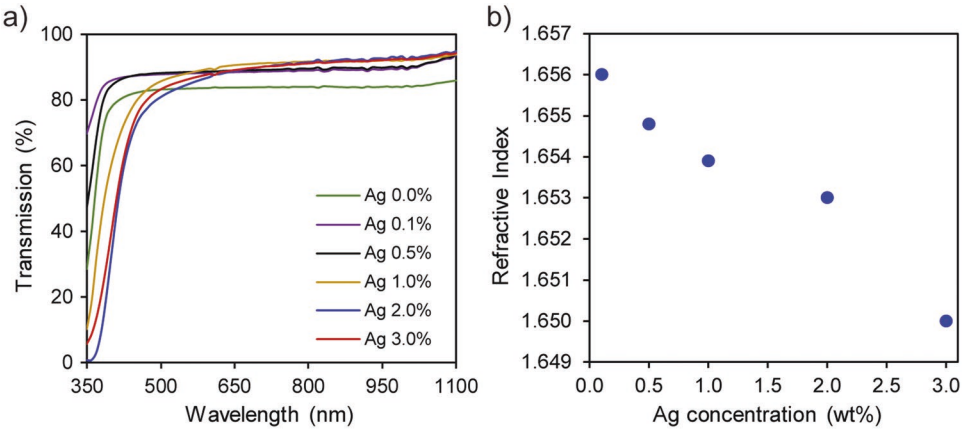

Figure 4. Optical characterization of metallo-dielectric waveguide arrays as a function of $AgSbF_6$ concentration. a) Transmission spectra. b) Refractive index of photocured NOA65+ $AgSbF_6$ formulations.

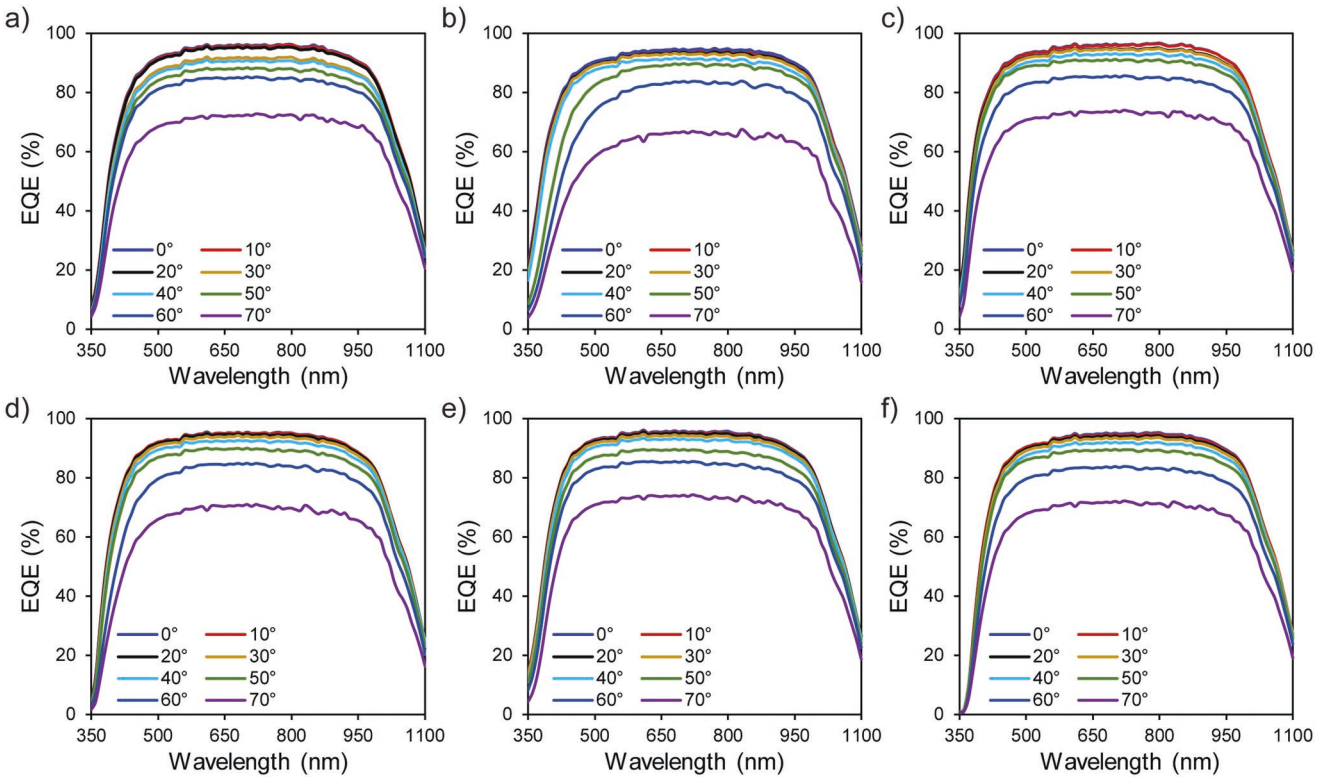

Figure 5. Efficiency spectra of encapsulated solar cells at different incident angles for waveguide arrays processed with a–f) 0%, 0.1%, 0.5%, 1.0%, 2.0%, and 3% $AgSbF_6$, respectively.

Figure 6 plots the average EQE as a function of incident angle for all encapsulants as well as the nominal percent difference with respect to the 0 wt% $AgSbF_6$ sample. $AgSbF_6$ concentrations from 0.1 to 3.0 wt% abate the decrease in EQE with increased incident angle (Figure 6a) leading to increases in the EQE, specifically for intermediate incident angles (30°–50°). The greatest increase is observed for 0.5 wt% $AgSbF_6$. The total EQE values for 0.5 wt% $AgSbF_6$ are greater over all angles. For small incident angles (0°–20°), with the exception of 0.5 wt% $AgSbF_6$, the efficiency drops are comparable to a 0 wt% sample, and this is also the case for certain samples at angles 60°–70°. Our previous studies show that the regular waveguide architecture results in a 10% increase in EQE over a uniform encapsulant over a range of angles (0°–40°). Hence, while certain $AgSbF_6$ concentrations do not out-perform the regular waveguide array, they still show an improvement over a uniform encapsulant.

Figure 7 provides current density to voltage (J–V) curves for the encapsulated solar cells for different incident angles over the range of $AgSbF_6$ concentrations explored. All plots show a monotonic decrease in the short circuit current densities with increase in incident angle, which is a natural trend, owing to increased shading loss from the greater apparent coverage of the contacts on the surface.[15b] While the EQE spectra show enhancements to the conversion efficiency in encapsulated cells, the electrical output, specifically the short circuit current density (J_{SC}), reveals more complex interactions. Specific Ag concentrations lead to increases in J_{SC} at particular incident angles. For example, waveguide arrays with 0.5 wt% $AgSbF_6$ increase J_{SC}, with respect to the 0 wt% sample, nominally by 3.5 mA cm^{-2} at 0° and by ≈1 mA cm^{-2} at 60° and 70°; however, J_{SC} is less or equal for intermediate angles. Waveguide arrays with 2 and 3 wt% $AgSbF_6$ increase J_{SC} by ≈0.5 mA cm^{-2} (max) in the angular range of 0°–30°. All other concentrations provide no enhancement to the current density, despite their apparent increases in efficiency for particular angular ranges shown in Figure 6b. The increase of 3.5 mA cm^{-2} is a promising enhancement to normal incidence operation, constituting a 9.9% increase to the short circuit current density, and the 1 mA cm^{-2} at the widest angle is attractive for preserving solar cell output at nonoptimal sunlight periods, such as morning, evening, or winter.

The variations in the EQE performance of the cells can be explained by the interactions of light with the waveguide and nanoparticle light scattering. For an incident angle of 0°, the forward scattering properties of the nanoparticles keep light directed toward the solar cell, enabling better conversion efficiency and greater current. For low nonnormally incident angles, the waveguide properties are suitable for collecting light, but the nanoparticles may scatter light out of the waveguide, which is not optimal and leads to reduced efficiency. With increasing angle, beyond the collection range of the waveguides, scattering becomes beneficial, as it imposes a redirecting effect, steering light otherwise outside of the acceptance range of the waveguides into it, thereby allowing for greater light collection. At even greater angles these collection effects can be sustained, particularly as observed for lower $AgSbF_6$ concentrations, thereby providing enhancement at very large incident angles. However, at greater concentrations, the

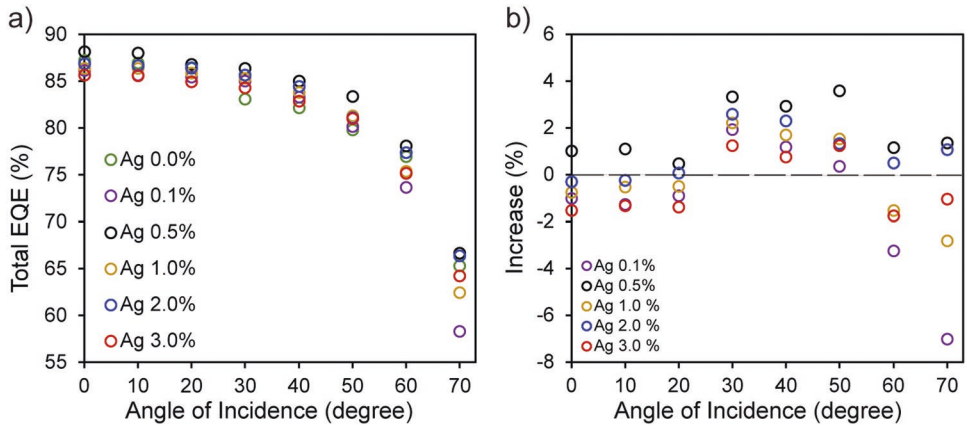

Figure 6. a) Total EQE measurements as a function of incident angle for waveguide arrays processed with different $AgSbF_6$ concentrations. b) Nominal increase in total EQE of metallo-dielectric waveguide arrays relative to a waveguide array with no Ag nanoparticles.

scattering effect might dominate, leading to reduced efficiency. It is also likely that the silver nanoparticles enable scattering of light to outside of the loss cone of the solar cell. Examining the combination of EQE and current measurements, waveguide arrays with 0.5 wt% $AgSbF_6$ provide the greatest enhancement to solar cell performance. Simulations on the combined optical waveguiding and scattering effects of this new encapsulant structure are currently underway, to provide further elucidation of the correlation between nanoparticle content and solar cell performance, and this will be reported in the future. Similar measurements on solar cells with laminated films show that, overall, the efficiency and current density were more stable and better solar performance was observed for directly processed encapsulants (see Supporting Information).

From a materials standpoint, this encapsulant resin formulation of a high index acrylate and low index silicone can perform better than industrial ethylene vinyl acetate (EVA) coatings in terms of durability, adhesion, transmittance, and cost, and can further address EVA's persistent discoloration.[22] Economically, the low concentration of silver precursor would yield only a marginal increase to the cost of the polymer resin formulation. Measurements on an encapsulated solar cell after 3 months

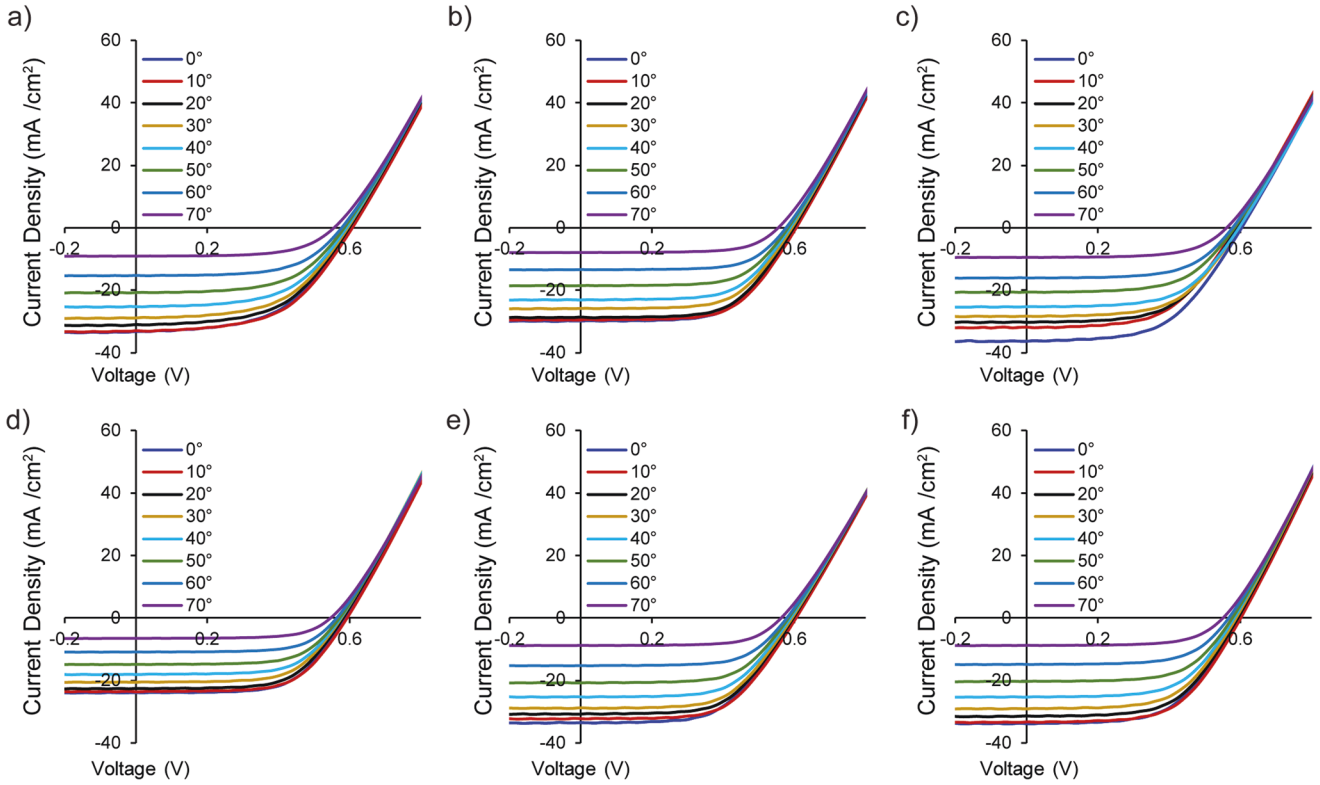

Figure 7. Performance of encapsulated solar cells. a–f) *J–V* curves at different incident angles for waveguide arrays processed with 0%, 0.1%, 0.5%, 1.0%, 2.0%, and 3.0% $AgSbF_6$, respectively.

showed no degradation in the solar cell performance as compared to its performance when the encapsulant was new (see Supporting Information), indicating the stability of the structures. Long-term stability tests are currently underway, and will be reported in the future.

3. Conclusion

Arrays of metallo-dielectric waveguides were fabricated from photoreactive thin-film resins consisting of a binary component blend of polymers and a silver salt as the metal source. The structures form through irradiation and self-trapping of UV optical beams, which drive the phase separation of the polymer components and the photochemical synthesis of silver nanoparticles. The structure comprises high refractive index polymer cores, with silver nanoparticles embedded in it (i.e., a metallo-dielectric), surrounded by a low refractive index polymer. The structures were tested as encapsulant materials for silicon solar cells to leverage their observed wide-angle light collection properties. Increases in both the conversion efficiency and the current output over a range of nonnormally incident angles are observed, and specific weight fractions of silver precursor lead to significant enhancements in conversion efficiency and current density. The results are promising, and further study is needed to elucidate the light-matter interactions to closely correlate the structure with solar cell performance, toward greater improvement.

4. Experimental Section

Materials: High refractive index NOA65 was purchased from Norland Products Inc., and low refractive index epoxide-terminated PDMS oligomer and silver hexafluoroantimonate(V) ($AgSbF_6$) were purchased from Sigma-Aldrich. The UV initiator (4-octyloxyphenyl) phenyliodonium hexafluoroantimonate (OPPI) was purchased from Hampford Research Inc. All chemicals were used without further purification.

Preparation of Photopolymerizable Media: Polymer blends were prepared by thoroughly mixing under dark conditions PDMS and NOA65 in a 1:1 by weight fraction (48 wt% each of total mixture) with OPPI (1.5 wt% of total mixture) and different weight fractions of $AgSbF_6$ (0.1–3.0 wt% of total mixture).

Irradiation of the Blends: The mixture was exposed to collimated UV light generated from a Xenon lamp source (≈30 mW cm^{-2}). The light was first transmitted through a chrome mask consisting of a square array of apertures of diameter 40 µm and spacing of 200 µm. Two approaches for encapsulation of the solar cells were explored. In the first approach, the resin was cast over the solar cell, and irradiated with the array of UV beams from above. This approach is herein referred to as direct processing. In the second approach, the encapsulant was synthesized separately, and then applied over the solar cell that had been first planarized with a layer of silicone (Sylgard 184). This approach is herein referred to as a lamination. All data for laminated encapsulants are shown in the Supporting Information.

Refractive Index Measurements: Refractive index values for photocured formulations were measured with an Abbe refractometer (Atago, NAR-1T SOLID).

Raman Volume Mapping: 3D composition maps of the Ag nanoparticle distribution were generated by 3D mapping of the material's Raman spectra, as described previously,[14] then rendering a 3D volume for a Raman peak for silver (994 cm^{-1}).

Optical Intensity Profiling: The transverse spatial intensity profile of light transmitted through the materials was captured with a charge-coupled device (CCD) camera, using an optics setup described previously.[23]

Solar Cell Measurements: EQE spectra and total EQE were measured and calculated, respectively, as described previously.[13a] A planar multicrystalline silicon screen-printed solar cell (5 cm × 5 cm × 0.5 mm) with a measured short circuit current density of 35.5 mA cm^{-2} was used in experiments. Current density–voltage (*J*–*V*) curves of encapsulated solar cells were collected under AM 1.5 G radiation using an ABB class solar simulator.

Supporting Information

Supporting Information is available from the Wiley Online Library or from the author.

Acknowledgements

The authors gratefully acknowledge funding from the American Chemical Society (PRF# 57332-DNI7), the National Science Foundation (CMMI-1751621), the 3M Foundation (Non-Tenured Faculty Award), as well as support from the College of Engineering and Computer Science at Syracuse University.

Conflict of Interest

The authors declare no conflict of interest.

Keywords

direct optical coating, polymers, silver nanoparticles, solar cells, waveguides

Received: April 21, 2019
Revised: July 1, 2019
Published online:

[1] T.-D. Cheng, Y.-P. Chen, P.-C. Chen, presented at Proc. 27th European Photovoltaic Solar Energy Conf. and Exhibition, Frankfurt, Germany, September **2012**.

[2] a) Q. Xu, L. Meng, X. Wang, *Appl. Opt.* **2019**, *58*, 2505; b) J. Jaus, H. Pantsar, J. Eckert, M. Duell, H. Herfurth, D. Doble, *IEEE Photovoltaic Spec. Conf.* **2010**, *35*, 979; c) R. Ebner, M. Schwark, B. Kubicek, G. Újvári, W. Mühleisen, C. Hirschl, L. Neumaier, M. Pedevilla, J. Scheurer, A. Plösch, A. Kogler, W. Krumlacher, H. Muckenhuber, presented at Proc. 28th European Photovoltaic Solar Energy Conf. Exhibition, Paris, France, September **2013**; d) I. Mingareev, R. Berlich, T. J. Eichelkraut, H. Herfurth, S. Heinemann, M. C. Richardson, *Opt. Express* **2011**, *19*, 11397.

[3] J. van Deelen, Y. Tezsevin, A. Omar, M. Xu, M. Barink, *MRS Adv.* **2017**, *2*, 3175.

[4] H. Lin, S. Biria, F.-H. Chen, I. D. Hosein, K. Saravanamuttu, *ACS Photonics* **2019**, *6*, 878.

[5] a) F. H. Chen, S. Pathreeker, J. Kaur, I. D. Hosein, *Opt. Express* **2016**, *24*, A1419; b) M. F. Schumann, M. Langenhorst, M. Smeets, K. Ding, U. W. Paetzold, M. Wegener, *Adv. Opt. Mater.* **2017**, *5*, 1700164.

[6] E. Van Kerschaver, G. Beaucarne, *Prog. Photovoltaics* **2006**, *14*, 107.

[7] Y. H. Jang, Y. J. Jang, S. Kim, L. N. Quan, K. Chung, D. H. Kim, *Chem. Rev.* **2016**, *116*, 14982.
[8] K. R. Catchpole, A. Polman, *Appl. Phys. Lett.* **2008**, *93*, 191113.
[9] V. E. Ferry, M. A. Verschuuren, H. B. T. Li, E. Verhagen, R. J. Walters, R. E. I. Schropp, H. A. Atwater, A. Polman, *Opt. Express* **2010**, *18*, A237.
[10] S. Mokkapati, F. J. Beck, R. de Waele, A. Polman, K. R. Catchpole, *J. Phys. D: Appl. Phys.* **2011**, *44*, 185101.
[11] Y. Y. Lee, W. J. Ho, J. J. Liu, C. H. Lin, *Jpn. J. Appl. Phys.* **2014**, *53*, 06JE11.
[12] D. M. Callahan, J. N. Munday, H. A. Atwater, *Nano Lett.* **2012**, *12*, 214.
[13] a) S. Biria, F.-H. Chen, I. D. Hosein, *Phys. Status Solidi* **2019**, *216*, 1800716; b) S. Biria, F. H. Chen, S. Pathreeker, I. D. Hosein, *Adv. Mater.* **2017**, *30*, 1705382.
[14] S. Biria, I. D. Hosein, *Macromolecules* **2017**, *50*, 3617.
[15] a) O. Korech, J. M. Gordon, E. A. Katz, D. Feuermann, N. Eisenberg, *Opt. Lett.* **2007**, *32*, 2789; b) M. F. Stuckings, A. W. Blakers, *Sol. Energy Mater. Sol. Cells* **1999**, *59*, 233; c) K. J. Weber, V. Everett, P. N. K. Deenapanray, E. Franklin, A. W. Blakers, *Sol. Energy Mater. Sol. Cells* **2006**, *90*, 1741.
[16] M. Sangermano, Y. Yagci, G. Rizza, *Macromolecules* **2007**, *40*, 8827.
[17] I. D. Hosein, H. Lin, M. R. Ponte, D. K. Basker, K. Saravanamuttu, presented at Renewable Energy and the Environment, Tucson, AZ, November **2013**.
[18] W. J. Ho, J. C. Lin, J. J. Liu, C. W. Yeh, H. J. Syu, C. F. Lin, *Materials* **2017**, *10*, E737.
[19] Y. Yagci, M. Sangermano, G. Rizza, *Macromolecules* **2008**, *41*, 7268.
[20] A. A. Askadskii, *Polym. Sci. U.S.S.R.* **1990**, *32*, 2061.
[21] B. E. A. Saleh, M. C. Teich, *Fundamentals of Photonics*, John Wiley & Sons, Inc., New York **2001**.
[22] J. H. Wohlgemuth, M. D. Kempe, D. C. Miller, presented at IEEE Photovoltaic Specialists Conf., Colorado, USA, June **2013**.
[23] a) S. Biria, P. P. A. Malley, T. F. Kahan, I. D. Hosein, *J. Phys. Chem. C* **2016**, *120*, 4517; b) I. D. Hosein, H. Lin, M. R. Ponte, D. K. Basker, M. A. Brook, K. Saravanamuttu, *Adv. Funct. Mater.* **2017**, *27*, 1702242.

